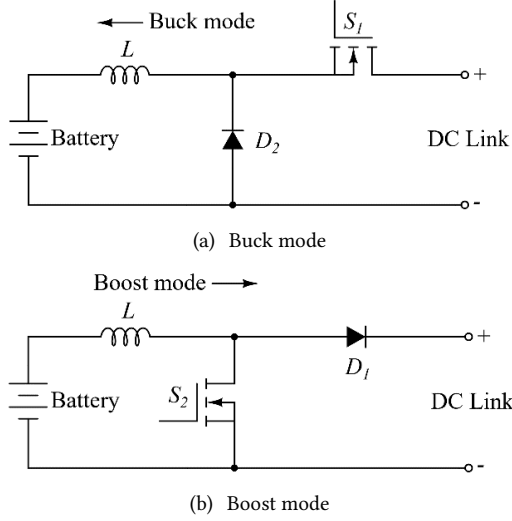


Digital Object Identifier: 10.37936/ecti-eec.2022201.246112



**Fig. 2:** Operation mode of the bidirectional converter; (a) buck mode and (b) boost mode.

of the inverter is considered on the low-voltage side. The circuit charges the current from the photovoltaic source more quickly when the battery value is lower (battery side). Since the current in the lower circuit is distributed swiftly on the high-voltage side, the proposed energy transfer system transmits power between the battery side and grid inverter. Moreover, the input voltage of the grid inverter will be controlled at the required rating.

## 2. CIRCUIT DESCRIPTION AND SIMULATION

### 2.1 Bidirectional DC-DC Converter

Fig. 1 shows a non-isolated bidirectional DC-DC converter using half-bridge topology to integrate buck and boost modes [18–19]. The basic operation of the converter is based on two different modes to transfer energy between low-voltage (battery) and high-voltage sources (DC link) depending on the system requirement.

#### 2.1.1 Buck mode

In this mode, switch  $S_1$  and diode  $D_2$  conduct according to the duty cycle ( $D$ ), while switch  $S_2$  and diode  $D_1$  remain off during the operation. To charge the battery, power is transferred from the higher voltage side to the lower voltage side. The circuit of this mode is shown in Fig. 2(a). Therefore, the voltage across the battery ( $V_{battery}$ ) can be expressed as

$$V_{battery} = DV_{dc \text{ link}}. \quad (1)$$

#### 2.1.2 Boost mode

In this mode, switch  $S_2$  and diode  $D_1$  conduct according to the duty cycle, while switch  $S_1$  and diode  $D_2$  remain off during the operation. The battery discharges as power is transferred from the lower to higher voltage side. The circuit of this mode is shown in Fig. 2(b). Therefore, the voltage across the DC link ( $V_{dc \text{ link}}$ ) can be expressed as

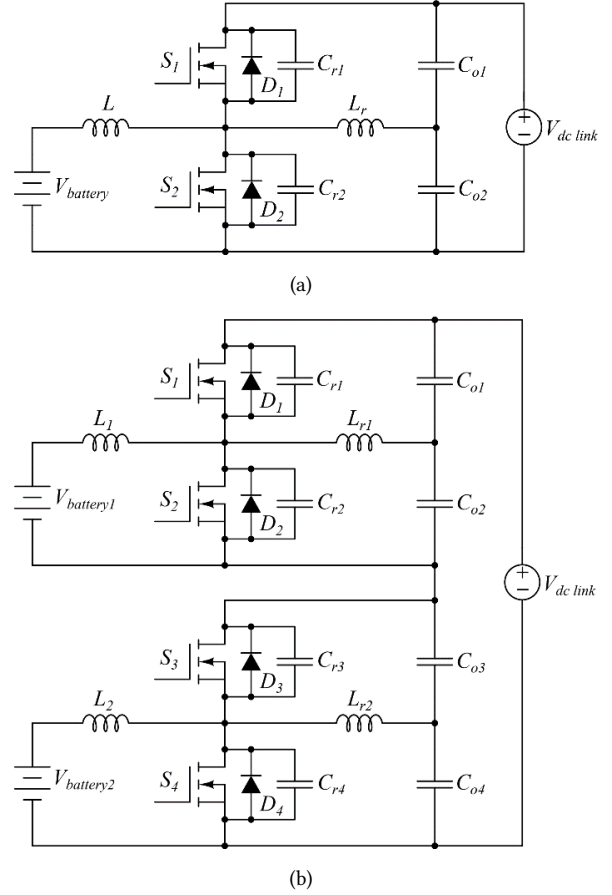


**Fig. 3:** (a) Soft switching topology and (b) series of connected soft switching converter circuits.

$$V_{dc \text{ link}} = \frac{V_{battery}}{1 - D}. \quad (2)$$

#### 2.1.3 Inductor calculation

The minimum inductance value ( $L_{min}$ ) is required to enable the converter to operate in continuous current mode (CCM). Therefore, the minimum inductance is calculated by

$$L_{min} = \frac{(1 - D)V_{battery}T_s}{2I_{battery}} \quad (3)$$

where  $I_{battery}$  is the current flowing through the battery and  $T_s$  the switching period.

## 2.2 Proposed Circuit Description

Due to the hard-switching operation, the bidirectional DC-DC converter shown in Fig. 1 exhibits significant losses. However, such losses can be reduced by replacing a resonant circuit that operates in a soft switching mode, as shown in Fig. 3(a). To increase the voltage level at the DC link, two converter circuit modules from Fig. 3(a) are connected in series as shown in Fig. 3(b). The voltage rating needs to be increased in order to study how the required voltage rating can be obtained in the

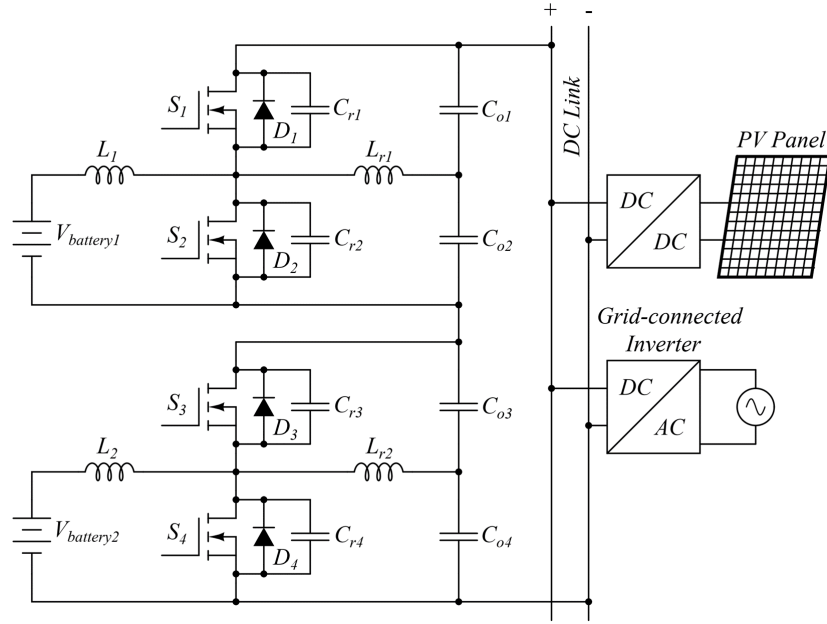


Fig. 4: Circuit configuration of the bidirectional resonant converter.

first place and develop a system for further increasing the high-voltage rating.

Hard-switching converters often incur losses during the process, resulting from the source of high-stress technological devices and considerable heat buildup. Inductors and capacitors are used to solve the problems outlined above. To eliminate energy loss, an  $LC$  resonant is employed to improve the converter circuit, operating with the same topology as a buck-boost converter. A resonant coil ( $L_r$ ) is added as a snubber circuit to protect the system from overcurrent. It is possible to reduce the losses in the built-in switch during operation. When switching devices are introduced to the converter circuit,  $S_1$ ,  $S_2$ ,  $S_3$ , and  $S_4$  can operate in zero-voltage conditions. The resonant circuit has various advantages, including lower cost. Moreover, it does not necessitate a circuit design requiring the addition of equipment or other components.

As presented in Fig. 4, the solar cell energy transfer system operates by connecting a bidirectional resonant converter circuit in series with a battery linked to the low-voltage side for transferring energy and maintaining a constant voltage on the grid inverter side. Switches  $S_1$  and  $S_2$  are set to operate simultaneously. Switch  $S_2$  is usually the first to turn on, causing the inductor to charge. Switches  $S_3$  and  $S_4$  in the converter circuit function in the same way. In practice, the voltage for this series-connected converter circuit can be increased twice, but in this research, a transformer is not used to enhance the system voltage. Since the transformer has a rather high magnetic field, the reliability of the circuit will be affected. It will operate in interleaved mode to help supply power to the system when two converter circuits are linked in series. To examine and achieve the optimal value for the cycle, the duty cycle

value starting at 50% is used in this research. If the duty cycle is set to a value that is either too high or too low, the circuit will malfunction and cause damage. The inductor ( $L_r$ ) in the bidirectional resonant converter is a very important component because it is responsible for storing and discharging energy. As a result, the output voltage level is higher than the input voltage level. The value of a resonant inductor can be calculated by

$$L_r = \left[ \frac{[\Delta V_o(\Delta V_o + 2V_o)] C_r}{I_o^2} \right]. \quad (4)$$

The inductor is a power-storage and distribution component. As a result, the output voltage level is higher than the input voltage level. The minimum inductance of the circuit can be calculated from Eq. (3) and the resonant capacitor from

$$C_r = \left[ \frac{L_r I_o^2}{\Delta V_o(\Delta V_o + 2V_o)} \right]. \quad (5)$$

While the switch device is turned on, the output capacitor of the circuit is responsible for storing the electric charge and supplying voltage to the load or discharging the electric charge. The electric charge operates when the switch device is switched off. Consequently, a capacitor capacity capable of withstanding a voltage equal to or greater than the output voltage must be chosen. The use of a large capacitor will help to reduce output voltage ripple ( $\Delta V_o$ ). The output capacitor can be calculated as

$$C_o = \frac{I_o D}{f_s \Delta V_o}. \quad (6)$$

When choosing capacitor values, the output voltage ripple will be reduced if a larger capacitance is utilized in the circuit. However, the capacitance must not be less than the calculated value.

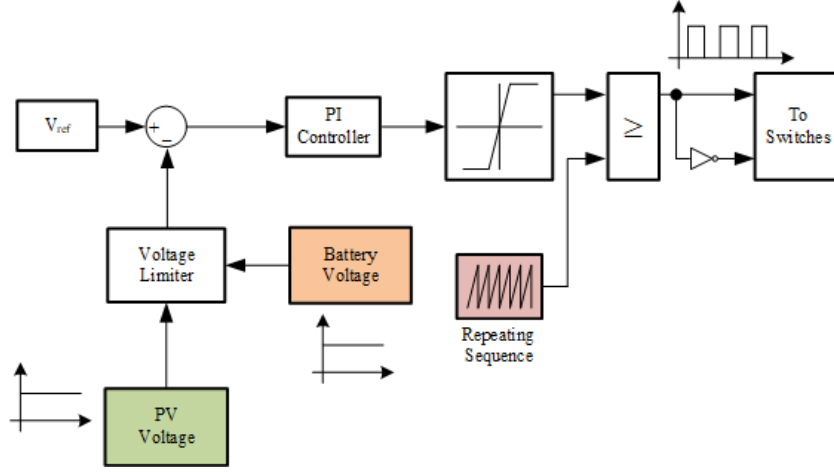


Fig. 5: Proposed feedback control circuit.

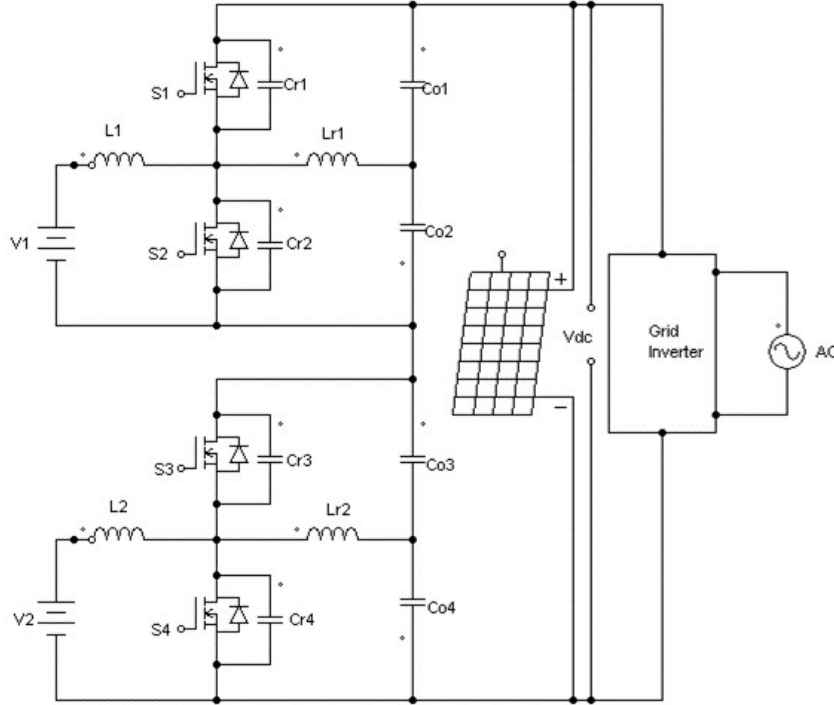


Fig. 6: Simulation model of the proposed converter.

### 2.3 Controller

The feedback control system of the converter circuit is shown in Fig. 5. It is a feedback circuit, controlling the high-voltage level (grid inverter side) at a constant level and the current with PI control. It connects the battery to this converter circuit to provide energy storage during the daytime with sufficient solar energy. The stored electrical energy in the battery can be used to supply the grid inverter system during the nighttime. The battery and PV voltages are measured and then sent to a voltage limiter for comparison with the reference voltage ( $V_{ref}$ ). The PI controller obtains an error value from the comparison value, which will be used to modulate the repeating sequence signal. The duty cycle of the driving signal for switches will be adjusted by the controller.

### 2.4 Simulation

The system model of the solar cell energy transfer system, connecting a bidirectional resonant converter in series, is shown in Fig. 6 and can be simulated by the PSIM computer program. The dc-link voltage ( $V_{dc}$ ) is regulated according to

$$V_{dc} = \left( \frac{V_1 + V_2}{D} \right) \quad (7)$$

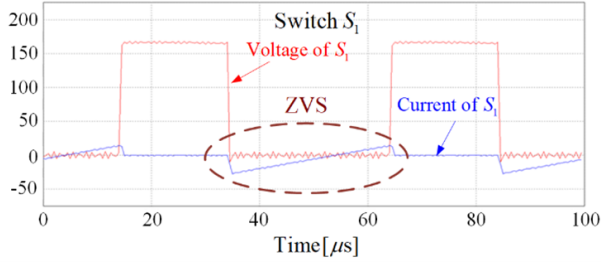
$$V_{dc} = \frac{V_1 + V_2 + \dots + V_n}{D} \quad (8)$$

$$V_1 = V_n \quad (9)$$

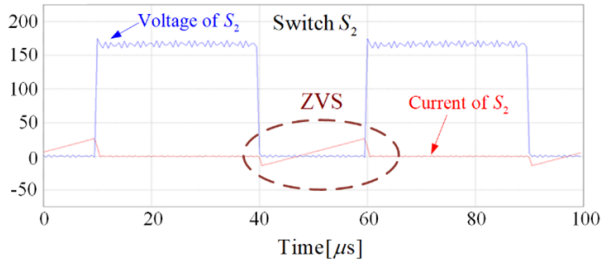
$$V_{dc} = \frac{nV_n}{D} \quad (10)$$

**Table 1:** Design specification and circuit parameters.

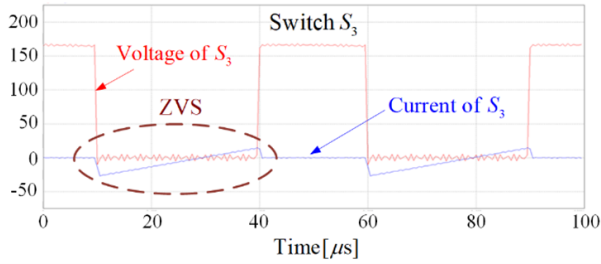
Parameter	Symbol	Value
DC-link voltage	$V_{dc\ link}$	48 V
Battery voltage	$V_{battery1,2}$	12 V
Switching frequency	$f_s$	35 kHz
Resonant capacitance	$C_{r1}, C_{r2}, C_{r3}, C_{r4}$	1 $\mu$ F
Resonant inductor	$L_{r1}, L_{r2}$	36 $\mu$ H
Output capacitance	$C_{o1}, C_{o2}, C_{o3}, C_{o4}$	220 $\mu$ F
Effective Inductance	$L_1, L_2$	2.6 mH
Dead time	$T_d$	2 $\mu$ s



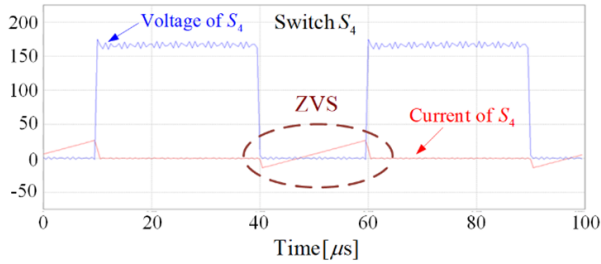
(a)



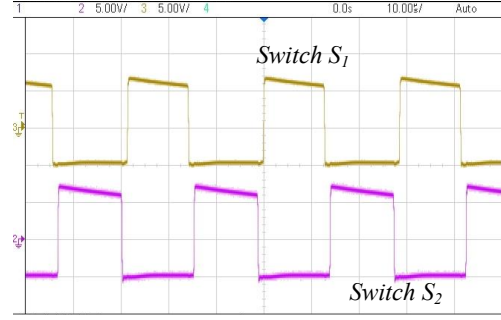
(b)



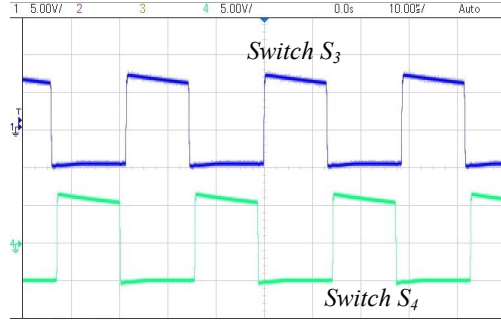
(c)



(d)

**Fig. 7:** Simulation waveform of switch voltage and current of (a)  $S_1$ , (b)  $S_2$ , (c)  $S_3$ , and (d)  $S_4$ .

(a)



(b)

**Fig. 8:** Experimental gate voltage pulse signal at (a)  $S_1$ ,  $S_2$  and (b)  $S_3$ ,  $S_4$ .

The inductor and resonant inductor current can be obtained by

$$i_L(t) = -\frac{V_o(t)}{L} + I_2 \quad (11)$$

$$i_{L_{r1,2}}(t) = \frac{V_{o1}(t)}{L} \quad (12)$$

### 3. SIMULATION AND EXPERIMENTAL RESULTS

The circuit parameters and design specifications for the simulation and experiment are shown in Table 1. Operating at zero-voltage switching (ZVS), the simulated voltage and current waveforms are shown in Fig. 7. Switches  $S_2$  and  $S_4$  are the first to be turned on. As can be observed, the voltage drops across the switches, and no current flows through them. When the voltage reaches zero, the current flow will begin to conduct the current in the negative diode phase. The switches will then begin to conduct the current in the positive range.

The gate drive signals of the switches are shown in Fig. 8, with  $S_2$  and  $S_4$  initially activated and  $S_1$  and  $S_3$  active only when  $S_2$  and  $S_4$  are deactivated.

To test the converter by connecting the battery to the converter circuit, the load will be powered by the series-connected bidirectional resonant converter as illustrated in Fig. 9. The load is initially set at a resistance of 1 k $\Omega$ .

The waveforms of voltage and current flowing through the MOSFET switches are shown in Figs. 10 and 11. At the bottom edge of the voltage waveform across the diode, there is zero voltage. The switch then conducts

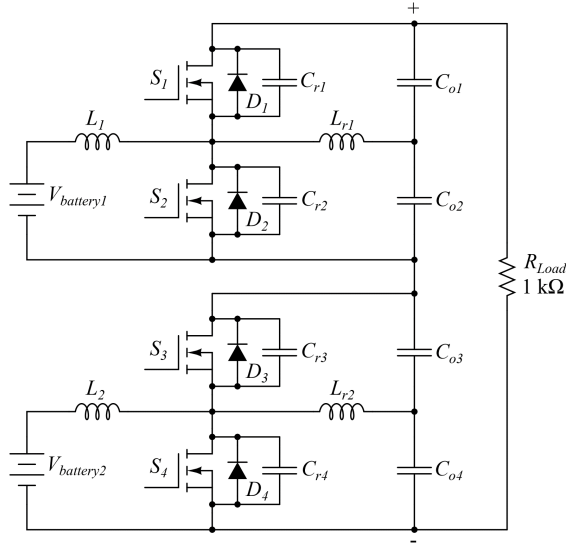


Fig. 9: Connecting the battery to converter for the  $R$  load.

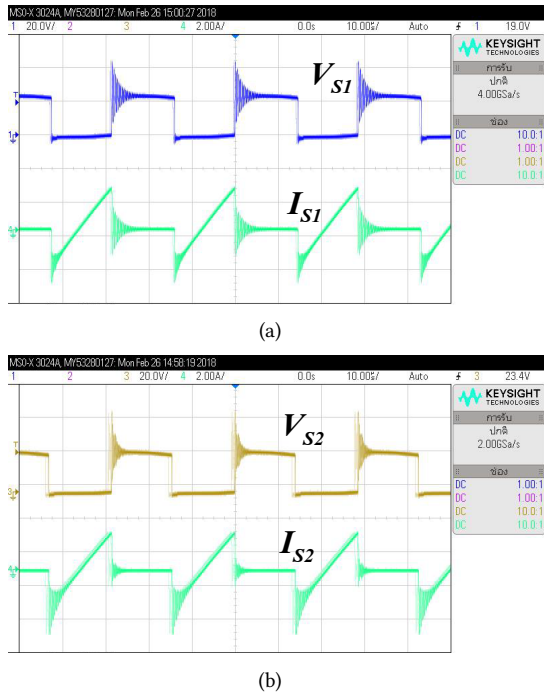


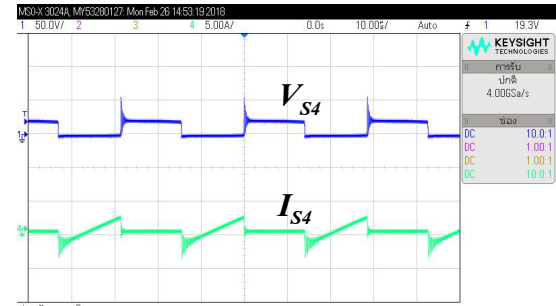
Fig. 10: Experimental voltage and current waveforms of (a)  $S_1$  and (b)  $S_2$ .

current, and the waveform derived from the simulation, as well as the experimental results, are both congruent with the theoretical conclusions. There is no power losses due to switching under the zero-voltage switching (ZVS) condition.

The actual operation test of the converter circuit power transfer system in buck and boost modes is shown in Figs. 12 and 13. The duty cycle values were adjusted at 50%. While the switches are turned on, the current and voltage waveforms are displayed. The current begins to overtake the negative diode current. When the voltage is zero, the switches will start to lead the positive current.

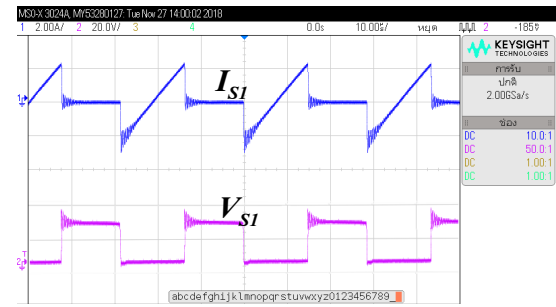


(a)

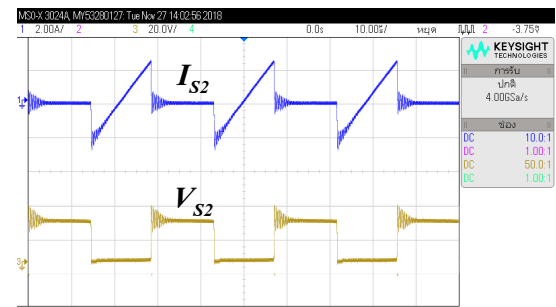


(b)

Fig. 11: Experimental voltage and current waveforms of (a)  $S_3$  and (b)  $S_4$ .



(a)

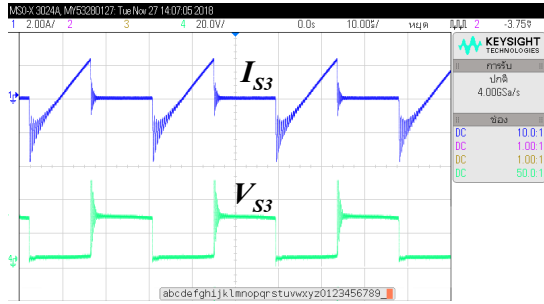


(b)

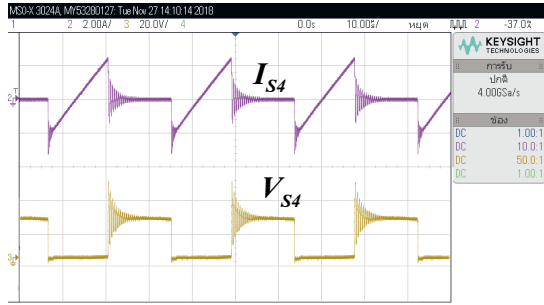
Fig. 12: Experimental voltage and current waveforms of (a)  $S_1$  and (b)  $S_2$  at 50% of the duty cycle.

The gate drive signal of the switches are illustrated in Fig. 8, switches  $S_2$  and  $S_4$  are begun first, and switches  $S_1$  and  $S_3$  can only be triggered once switches  $S_2$  and  $S_4$  are stopped. As can be seen in Figs. 12 and 13, no current will flow through the switch while the voltage is applied across it. Current will only flow through the switch if the voltage is zero. Current will begin to flow through





(a)



(b)

**Fig. 13:** Experimental voltage and current waveforms of (a)  $S_3$  and (b)  $S_4$  at 50% of the duty cycle.

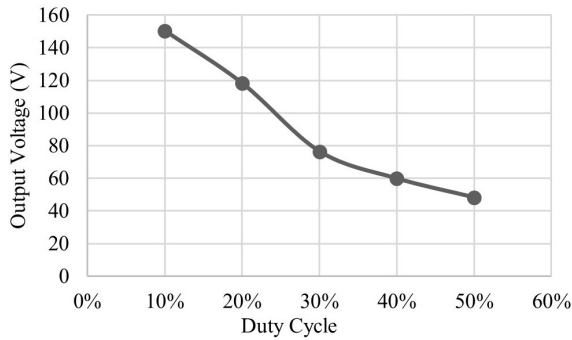
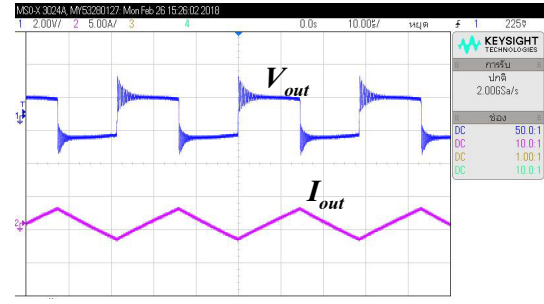


**Fig. 14:** Relationship between the output voltage and duty cycle.

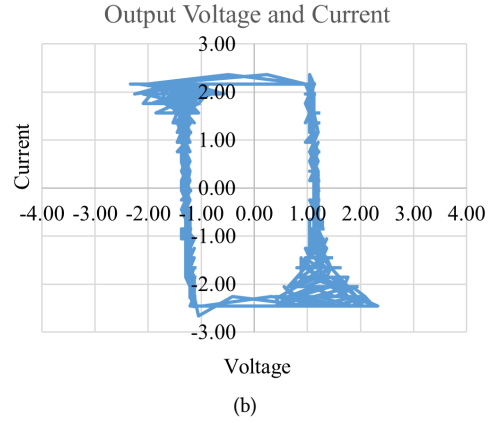
the switch during the negative diode initially. After that, the switch's voltage is zero. The deadtime is about  $2 \mu s$ .

Fig. 14 shows the relationship between output voltage and duty cycle. The output voltage is high when the duty cycle value is low. The output voltage of 150.4 V can be measured by experimenting with a 10% alteration in the duty cycle. The output voltage is low when the duty cycle is high. The output voltage is 48.2 V when the duty cycle is reduced by 50%.

To investigate circuit saturation, the phase-plane trajectories of the output current and voltage are shown in Figs. 15 and 16. The output voltage of the half-bridge inverter has a square waveform, while the output current has a triangular waveform. The prototype of the series-connected bidirectional resonant converter is shown in Fig. 17.

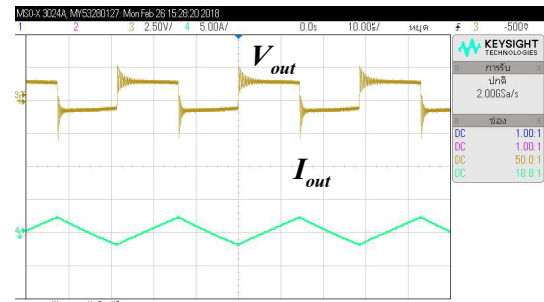


(a)

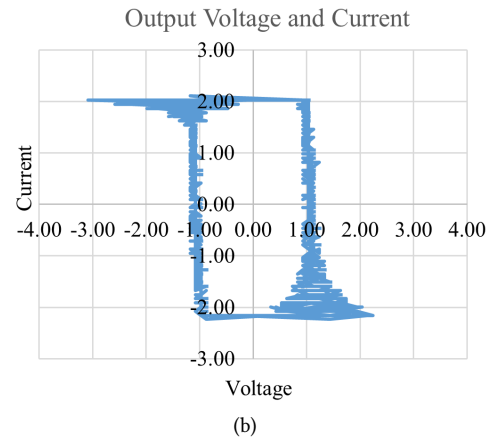


(b)

**Fig. 15:** (a) Experimental voltage and current waveforms of output voltage and current and (b) phase-plane trajectory plot of the converter module I.



(a)



(b)

**Fig. 16:** (a) Experimental voltage and current waveforms of output voltage and current and (b) phase-plane trajectory plot of the converter module II.



Fig. 17: Prototype of bidirectional resonant converter.

#### 4. CONCLUSION

A bidirectional resonant converter is proposed in this paper for asymmetrical duty cycle control and frequency control. Experiments on a solar cell energy transfer system using series-connected bidirectional resonant converters yield promising results. The circuit control is investigated and assessed using an experiment connecting batteries and solar cells. The simulation results will be implemented and the data changed accordingly so that it can be used in practical investigations. The testing results reveal that the output voltage of the grid-connected inverter is 48.2 V at a duty cycle of 50%. The output voltage of the grid-connected inverter can be increased to 150.4 V by decreasing the duty cycle by 10%. As a result, the bidirectional resonant converter can efficiently transmit energy and adjust the grid inverter's input voltage.

#### REFERENCES

- [1] J. Davies and P. Simpson, *Induction Heating Handbook*. New York, NY, USA: McGraw-Hill, 1979.
- [2] W. D. Stanley, *Operational Amplifiers with Linear Integrated Circuits*, 3rd ed. New York, NY, USA: Merrill, 1994, pp. 29–32.
- [3] J. M. Jacob, *Industrial Control Electronics: Applications and Design*. Singapore: Simon & Schuster, 1995, pp. 296–297.
- [4] H. Koertzen, J. van Wyk, and J. Ferreira, “Design of the half-bridge, series resonant converter for induction cooking,” in *Proceedings of PESC '95 - Power Electronics Specialist Conference*, 1995, pp. 729–735.
- [5] D. Pimentel, A. Cheriti, M. B. Slima, and P. Sicard, “Pulse density modulation pattern optimization using genetic algorithms,” in *32nd Annual Conference on IEEE Industrial Electronics (IECON 2006)*, 2006, pp. 1655–1660.
- [6] E. Dede, V. Esteve, J. Garcia, A. Navarro, and J. Carrasco, “On the design of high frequency series resonant converters for induction heating applications,” in *Proceedings of IECON '93 - 19th Annual Conference of IEEE Industrial Electronics*, 1993, pp. 1303–1307.
- [7] T. Nussbaumer, M. Baumann, and J. W. Kolar, “Comprehensive design of a three-phase three-switch buck-type PWM rectifier,” *IEEE Transactions on Power Electronics*, vol. 22, no. 2, pp. 551–562, Mar. 2007.
- [8] S. Chudjuarjeen and C. Koompai, “A high-frequency induction cooker using quasiresonant converter,” in *2007 4th International Conference on Electrical Engineering/Electronics, Computer, Telecommunications and Information Technology (ECTI-CON 2007)*, 2007, pp. 378–381.
- [9] S. Chudjuarjeen and C. Koompai, “Asymmetrical control with phase lock loop for induction cooking appliances,” in *2008 5th International Conference on Electrical Engineering/Electronics, Computer, Telecommunications and Information Technology (ECTI-CON 2008)*, 2008, pp. 1013–1016.
- [10] N.-J. Park, D.-Y. Lee, and D.-S. Hyun, “A power-control scheme with constant switching frequency in class-d inverter for induction-heating jar application,” *IEEE Transactions on Industrial Electronics*, vol. 54, no. 3, pp. 1252–1260, Jun. 2007.
- [11] L. de Vicuna, M. Castilla, J. Miret, J. Matas, and J. Guerrero, “Sliding-mode control for a single-phase AC/AC quantum resonant converter,” *IEEE Transactions on Industrial Electronics*, vol. 56, no. 9, pp. 3496–3504, Sep. 2009.
- [12] M.-K. Nguyen, Y.-G. Jung, and Y.-C. Lim, “Single-phase AC-AC converter based on quasi-z-source topology,” *IEEE Transactions on Power Electronics*, vol. 25, no. 8, pp. 2200–2210, Aug. 2010.
- [13] X. P. Fang, Z. M. Qian, and F. Z. Peng, “Single-phase z-source PWM AC-AC converters,” *IEEE Power Electronics Letters*, vol. 3, no. 4, pp. 121–124, Dec. 2005.
- [14] S. Chudjuarjeen, A. Sangswang, and C. Koompai, “An improved LLC resonant inverter for induction-heating applications with asymmetrical control,” *IEEE Transactions on Industrial Electronics*, vol. 58, no. 7, pp. 2915–2925, Jul. 2011.
- [15] S. Yachiangkam, A. Sangswang, S. Naetiladdanon, C. Koompai, and S. Chudjuarjeen, “Steady-state analysis of ZVS and NON-ZVS full-bridge inverters with asymmetrical control for induction heating applications,” *Journal of Power Electronics*, vol. 15, no. 2, pp. 544–554, Mar. 2015.
- [16] J. Jittakort, A. Sangswang, S. Naetiladdanon, C. Koompai, and S. Chudjuarjeen, “Full bridge resonant inverter using asymmetrical control with resonant-frequency tracking for ultrasonic cleaning applications,” *Journal of Power Electronics*, vol. 17, no. 5, pp. 1150–1159, Sep. 2017.
- [17] S. Nilboworn, K. Mahamad, W. Sangchay, and P. Kongrueang, “Edge effect and its influence on the adjacent cavities in a composite insulator,” *UTK*



*Research Journal*, vol. 14, no. 1, pp. 23–29, 2020.

- [18] K. Suresh and D. R. Arulmozhiyal, "Design and implementation of bi-directional DC-DC converter for wind energy system," *Circuits and Systems*, vol. 07, no. 11, pp. 3705–3722, 2016.
- [19] R. Pramanik and B. Pati, "Modelling and control of a non-isolated half-bridge bidirectional DC-DC converter with an energy management topology applicable with EV/HEV," *Journal of King Saud University - Engineering Sciences*, 2021.



**Nathabhat Phankong** received his B. Eng. (second-class honors) and M. Eng. degrees in electrical engineering from King Mongkut's University of Technology Thonburi (KMUTT), Thailand in 1999 and 2003, respectively, and his Ph.D. degree in electrical engineering from Kyoto University, Japan in 2010. He is currently a lecturer in the Department of Electrical Engineering, Rajamangala University of Technology Thanyaburi, Thailand. His research interests are mainly in

power electronic systems and conversion.



**Saichol Chudjuarjeen** received his B. Eng. degree in electrical engineering from Mahanakorn University of Technology (MUT), Thailand in 2000, M. Eng. degree in electrical engineering, and Ph.D. degree in electrical and computer engineering from King Mongkut's University of Technology Thonburi (KMUTT), Thailand in 2004 and 2011, respectively. He is currently a lecturer in the Department of Electrical Engineering, Rajamangala University of Technology Krungthep, Thailand. His research interests mainly involve high frequency resonant inverters for induction heating, current source and voltage source inverters, and control of power electronic systems.